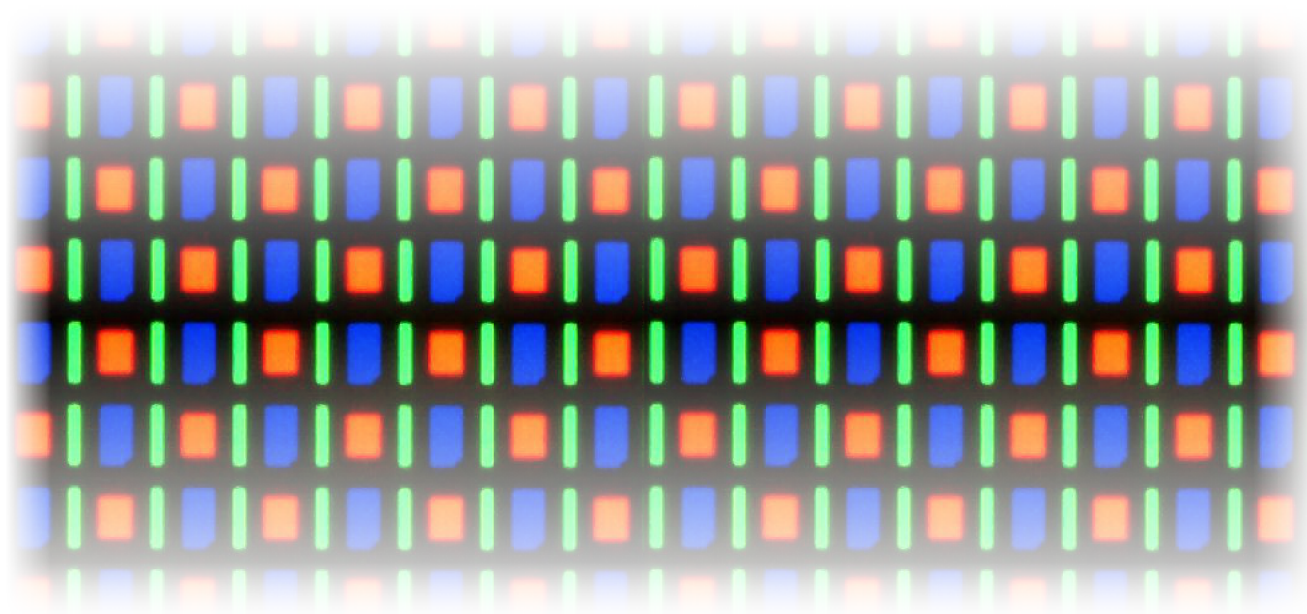Thermally Activated Delayed Flourescence (TADF)

Thermally Activated Delayed Flourescence (TADF)

Given nowadays popularity of smartphones and many other potential applications, OLED materials and organic electronics are a very active field of research and industrial developments.

The following tutorial illustrates how advanced electroluminescence phenomena of OLED materials can be simulated and studied. After a more general introduction to the topic, the approach presented below is largely based on the following recent publications:

P.K. Samanta, D. Kim, V. Coropceanu, J.-L. Brédas *Up-Conversion Intersystem Crossing Rates in Organic Emitters for Thermally Activated Delayed Fluorescence: Impact of the Nature of Singlet vs Triplet Excited States*, J. Am. Chem. Soc. 139, 4042-4051 (2017).

A broader overview on the topic can be found for example in

Y.Olivier, B. Yurash, L. Muccioli, G. D'Avino, O. Mikhnenko, J. C. Sancho-García, C. Adachi, T.-Q. Nguyen, D. Beljonne *Nature of the singlet and triplet excitations mediating thermally activated delayed fluorescence*, Phys. Rev. Materials 1, 075602 (2017).

and

SCM

> ❗ **Note**
>
> This tutorial illustrates the modeling of TADF on the example of a realistic dye molecule. Expect several hours of computation time for each single-point evaluation.

General Remarks on Modelling OLED Emitters

Electronic Structure of OLED Materials

OLED devices typically consist of a thin layer of a host material which is doped with an organic (or metalorganic) emitter material. Applying an electric voltage across such semiconductor layers results in free electrons and electron holes, so-called charge carriers, travelling through the material. When these charge carriers recombine, strongly bound electron-hole pairs, so-called excitons are formed, which are entirely localized on a single emitter molecule and thereby correspond to electronic excitations.

As free electrons (and holes) are equally likely to be created with spin up or spin down configurations, 75% of the formed excitons emerge in a triplet state (total spin S = 1) while 25% are found in a singlet state (S = 0).
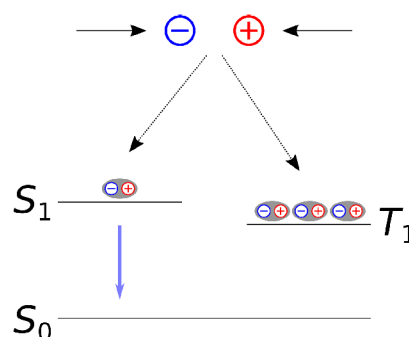

Fig. 11 Mechanism of first generation OLED emitters involving a flourescent decay path with a 25% maximum theoretical quantum yield.

This spin statistics negatively affects the quantum efficiency of an OLED material, hence on the proportion of electron-hole pairs that successfully undergo a radiative decay in to the ground state S_0 and emit a photon. A direct de-excitation from T_1 to S_0 is spin-forbidden in a non-relativistic theory. In the absence of any spin-orbit coupling effects in the dye, a radiative $T_1 \rightarrow S_0$ emission becomes very unlikely and light is only be emitted from a flourescent $S_1 \rightarrow S_0$ transition.

To address this problem a second generation of OLED emitters was developed involving OLED dyes containing heavy element atoms. Electrons in the valence shells of such atoms (e.g. Iridium)

$T_1 \rightarrow S_0$ decay and emit light.
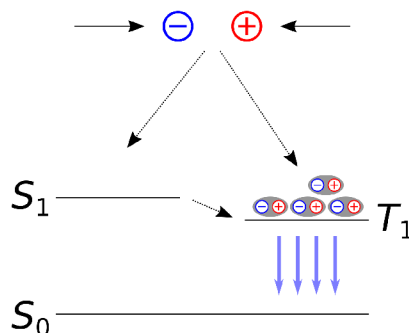
Fig. 12 Second generation OLED dyes rely on intersystem crossing to convert all excitons into a triplet state from which phosphorescent emissions occur.

While SOC-based emitters can reach quantum efficiencies of nearly 100%, the presence of long-living triplet states can cause chemical degradations. This tendency increases with the energy difference to the ground state (and thus with the frequency of the emitted light). As a result no stable, long-lasting OLED materials to deep blue light have been found as of yet. Apart from that, SOC-based dyes involve relatively rare and expensive heavy elements which significantly increases their costs.

These disadvantages motivated the development of third generation OLED materials: Dye molecules in which the states S_1 and T_1 are close in energy and (to some degree) vibrationally coupled, can exhibit a phenomenon known as thermally activated delayed flourescence (TADF). Using emitter molecules specifically tailored to maximize TADF, this effect can be exploited to avoid the degradation problems of SOC-based emitters. In addition, TADF occurs in purely organic dyes so that these third generation OLED emitters do not require expensive heavy metal elements.

TADF involves a reverse intersystem crossing (RISC) process, in which S_1 states are populated from T_1 levels. This is followed again by a normal flourescent transition $S_1 \rightarrow S_0$ and allows for light emissions with nearly 100% quantum yields.
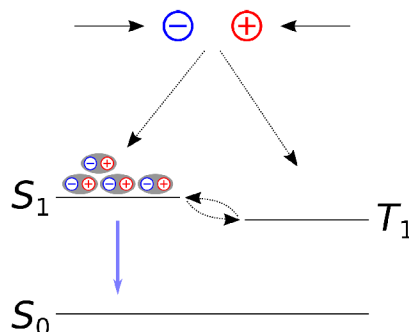
Fig. 13 The thermally assisted reverse intersystem crossing mechanism in third generation OLED

SCM

RISC competes with other processes such as the $S_1 \rightarrow T_1$ intersystem crossing. However, if non-radiative paths are negligible, k_{RISC} represents the rate-determining factor for TADF.

TADF represents a rather complex process and k_{RISC} has been shown to be strongly affected by various individual properties of a given dye material:

- singlet-triplet gap $\Delta E_{\mathrm{ST}} = E(S_1) - E(T_1)$
- spin-orbit interactions
- vibrational couplings between different electronic states
- solvent effects

Each of these aspects will be addressed in the following.

## Computational Description of TADF 1: Electronic Structure

A small singlet-triplet gap $\Delta E_{\mathrm{ST}} = E(S_1) - E(T_1)$ is essential for the RISC process. Indeed, the reverse intersystem crossing rate k_{RISC} is very sensitive regarding ΔE_{ST}, so that this quantity has to be predicted very precisely. Because of the required accurate electronic structure descriptions of excited states and their tiny energy differences, computational studies of TADF processes can be quite challenging for practical applications. As TADF dyes typically consist of hundreds of atoms, time-dependent density functional theory (TDDFT) often is the only computationally viable approach still accurate enough for modelling TADF processes.

To perform such TDDFT calculations, a suitable DFT approximation (i.e. exchange-correlation functional) needs to be chosen. Indeed, this is nontrivial question in itself. TDDFT results based on standard density functional approximations are inherently plagued by the self-interaction error. For the charge-transfer (CT) excitations typically found in OLED emitters such self-interaction effects cause spurious artifacts in the energies and electronic structure of excited states. While hybrid DFT methods ameliorate self-interaction errors, the excitation energies and electronic coupling parameters of TADF emitters are very sensitive regarding the amount of exact exchange incorporated in a given hybrid DFT approximation.

In range-separated hybrid (RSH) DFT methods the amount of exact exchange increases with the electron-electron distance. In many RSH approximations this used to restore the correct long-range asymptotic behavior of the corresponding potential. Their proper asymptotic behavior renders RSH methods potentially more accurate for the description of electronic excitations. The range-separation of RSH methods is controlled by and additional parameter ω, which corresponds to the inverse distance of the midpoint of the switching function between short- and long-range terms. The parameter ω can be tuned for a given emitter material to improve the

SCM

Excited States Geometry Optimizations

Following Samanta et al., we use TDDFT calculations in the Tamm-Dancoff approximation (TDA) to describe the TADF process in 1,2,3,5-tetrakis(carbazol-9-yl)-4,6-dicyanobenzene (4CzIPN), a typical TADF emitter.
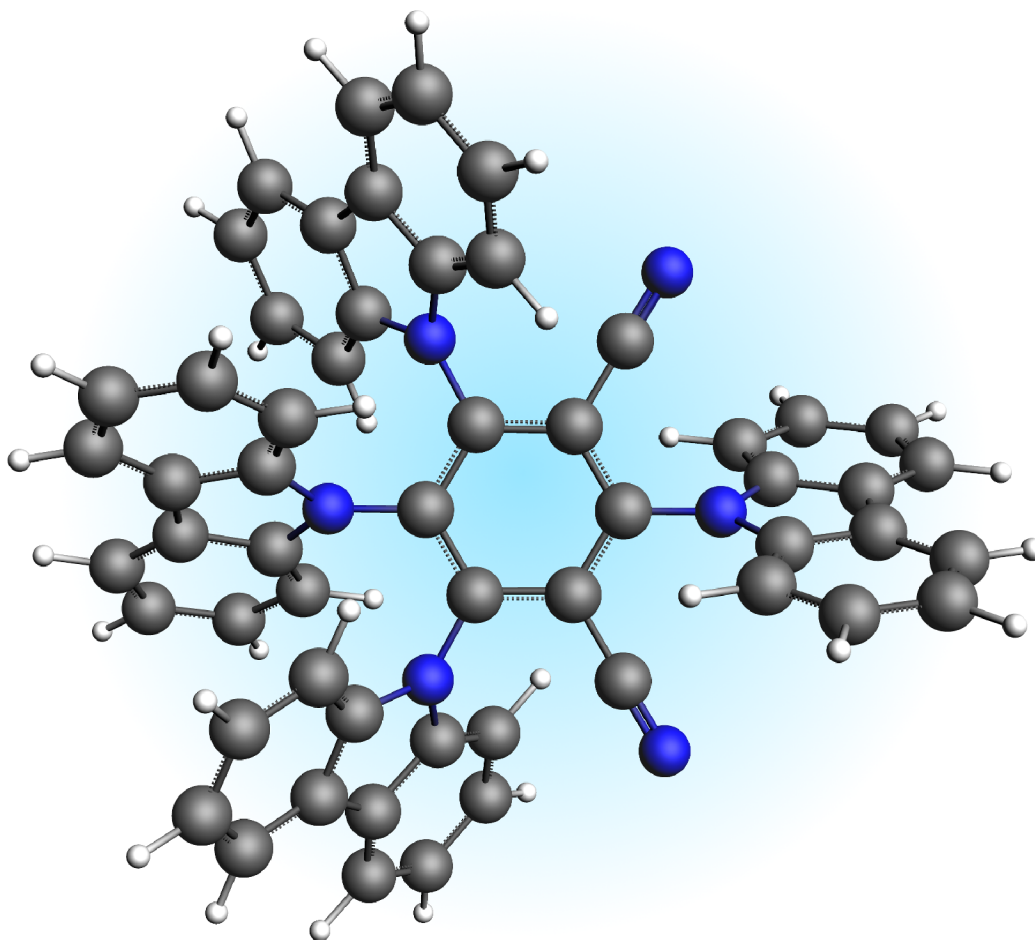
Fig. 14 1,2,3,5-tetrakis(carbazol-9-yl)-4,6-dicyanobenzene (4CzIPN)

Thereby we use the range-separated LCY-PBE functional, which employs a Yukawa potential to realize the switching function between long- and short-range terms. The sharpness of the Yukawa potential is controlled by the parameter γ, for which a value of 0.22 is used in the following.

🛈 **Note**

The value $\gamma = 0.22$ is the result of the RSH-tuning prescription of Karolewski et al. for the 4CzIPN molecule. Thereby the difference between the ionization potential and the HOMO energy is simultaneously minimized for a neutral and anionic system. Please follow the advanced tutorial tuning the range separation for range separated hybrids. Note, that γ is

SCM

To model the TADF process of 4CzIPN properly, the geometry of the system needs to be relaxed for all three relevant electronic states, S_0, S_1, and T_1, respectively. We can do this from GUI with ADF with the following settings:

Download the 4CzIPN structure ⬇ here

Start ADFinput

Load the structure with **File → Import Coordinates...**

In the **Main** panel:

Task: → Geometry Optimization

XC-Functional → Range Separated → LCY PBE

Click on the **...** button left of the **XC-Functional** field

Enter **Gamma:** 0.22

Return to **Main** panel

Relativity → Scalar

Basis set → TZP

Frozen core → None

Numerical quality → Good

Click on **Model** panel and select **Solvation**

Solvation method: → COSMO

COSMO solvent → Toluene

Save the input **File → Save as...** under e.g. *4CzIPN_GSopt.adf*

A few more additional options are needed to define the excited states geometry optimizations. In the case of the S_1-optimization:

In the window with the previously created *4CzIPN_GSopt.adf* file still open:

Properties → Excitations (UV/Vis), CD

Type of excitations: → SingletOnly

TDA: → Yes

Number of excitations: → 2

Calculate: → NTOs

Calculate: → Charge transfer descriptors

Properties → Excited State Geometry

Excitation: enter *1A*

Analogously for the T_1-state:

> **Properties → Excitations (UV/Vis), CD**
>
> **Type of excitations: → TripletOnly**
>
> **TDA: → Yes**
>
> **Number of excitations: → 2**
>
> **Calculate: → NTOs**
>
> **Calculate: → Charge transfer descriptors**
>
> **Properties → Excited State Geometry**
>
> **Excitation:** enter *1A*
>
> **Spin type → Triplet**
>
> Save the input **File → Save as...** under e.g. *4CzIPN_T1opt.adf*

We are now ready to run all three optimization jobs. Note that, for a system like 4CzIPN a excited states geometry optimization with RSH can take multiple hours. For your convenience, the relaxed structures for the S_0, S_1, and T_1 states, respectively as well as the corresponding input scripts can be downloaded here:

❶ See also

- ⬇ TADF_4CzIPN_GS.xyz 4CzIPN ground state structure
- ⬇ TADF_4CzIPN_S1.xyz 4CzIPN S_1 structure
- ⬇ TADF_4CzIPN_T1.xyz 4CzIPN T_1 structure
- ⬇ 4CzIPN_GO_GS.run run script ground state optimization
- ⬇ 4CzIPN_exGO_S1.run run script S_1 optimization
- ⬇ 4CzIPN_exGO_T1.run run script T_1 optimization

After these optimizations are concluded, the respective minimum energies of the states can be extracted at the end of the logfile:

```
<Feb15-2019> <23:02:54>   Converged.
<Feb15-2019> <23:03:11>     Bond Energy           -33.75755925 a.u.
<Feb15-2019> <23:03:11>     Bond Energy          -918.58992548 eV
<Feb15-2019> <23:03:11>     Bond Energy    -21183.19       kcal/mol
<Feb15-2019> <23:03:11>   Excited state energy (ground + excitation energy) for: 1A(Singlet-Triplet)
<Feb15-2019> <23:03:11>     Excited State Energy:                -33.67699976 a.u.
<Feb15-2019> <23:03:11>     Excited State Energy:               -916.39779022 eV
<Feb15-2019> <23:03:11>     Excited State Energy:          -21132.64       kcal/mol
<Feb15-2019> <23:03:12>   NORMAL TERMINATION
<Feb15-2019> <23:03:14>   END
```

From there we can extract the following energy differences (neglecting vibrational contributions

SCM
Free trial

$E_{S1} - E_{S0}$	$E_{T1} - E_{S0}$	$\Delta E_{ST} = E_{S1} - E_{T1}$
2.55 eV	2.39 eV	0.16 eV

The result is somewhat different from the results (ΔE_{ST} = 0.01 eV) of the original paper due to the different electronic structure description used therein. Compared to the experimental value of ΔE_{ST} = 0.1 eV, the difference is however smaller and we will use our computed results of 0.16 eV in the subsequent calculations of this tutorial.

The output file provides the charge transfer descriptors according to the prescription of Plasser and Lischka, which are obtained from transition density matrices.

```
1: 197a       -> 215a        0.0002
1: 204a       -> 207a        0.0002
1: 205a       -> 242a        0.0002

   NTO weight: 0.9941
      occ:   0.9755 205a:1        -0.1434 188a:1        -0.1317 193a:1
      virt: -0.9996 206a:1         0.0187 245a:1        -0.0160 221a:1

   Descriptors (based on Plasser, Lischka, et al.)
      CT_AT =    0.8969      R_HE  =    4.6809
   Descriptors (Peach, Tozer, et al.)
      LAMBDA =   0.3919      R_HE  =    1.6717
```

For the T_1 state we find a charge transfer (CT) character of 90% with an average electron-electron hole distance (R_HE) of 4.7 Å, while in the case of S_1 the CT character amounts to 94% with an average of 5 Å between the excited electron and electron hole. Note, that such high CT characters and electron-hole distances are a direct consequence of the design principles of typical OLED emitters featuring well-separated electron donor and acceptor groups. In consequence, these excited states also exhibit a relatively small exchange energy, which contributes most to the small ΔE_{ST} value computed above from TDDFT excitation energies.

Vertical Absorption

Following Samanta et al. and to analyze the system further, we compute vertical excitations at the ground state geometry to obtain the absorption spectrum of 4CzIPN. Note, that these results do not enter the calculation of the RISC rate but rather serve as an additional assessment of the accuracy of the description employed here. Regarding most aspects this is done analogously to the previous calculations. The main differences are that we now treat the excitations in a spin-orbit description which allows for pure spin-states (i.e. no spin contamination). Furthermore, the response of the solvation model is ignored as the solvent molecules cannot rearrange within the short timespan of a vertical excitation; a better

Open a new instance of ADFinput

Load the previously optimized GS structure with **File → Import Coordinates...**

In the **Main** panel:

Task: → Single Point

XC-Functional → Range Separated → LCY PBE

Click on the **...** button left of the **XC-Functional** field

Enter **Gamma:** 0.22

Return to **Main** panel

Relativity → Scalar

Basis set → TZP

Frozen core → None

Numerical quality → Good

Click on **Model** panel and select **Solvation**

Solvation method: → COSMO

COSMO solvent → Toluene

Click on **Details** panel and select **COSMO**

Untick **Include response in TDDFT**

Click on **Properties** and select **Excitations (UV/Vis), CD**

Type of excitations: → Spin-Orbit (Perturbative)

TDA: → Yes

Number of excitations: 5

Calculate: → NTOs

Calculate: → Charge transfer descriptors

Save the input **File → Save as...** under e.g. *4CzIPN_GS_VA.adf*

❶ See also

- ⬇ 4CzIPN_VA.run run script vertical absorption calculation

After completing this calculation, we open the results with ADFoutput and search for the results with **Response Properties → All Spin-Orbit Coupling Excitation Energies**:

```
 2:      0.09372      2.55025      0.7248E-09     4.889     A
 3:      0.09372      2.55025      0.1266E-08     2.798     A
 4:      0.10037      2.73109      0.1514E-05    0.2041E-02  A
 5:      0.10037      2.73109      0.2371E-08     1.303     A
 6:      0.10037      2.73109      0.1645E-07    0.1879     A
 7:      0.10164      2.76580      0.8882E-01    0.3392E-07  A
 8:      0.10592      2.88216      0.1760E-09    15.76      A
 9:      0.10592      2.88216      0.1001E-06    0.2772E-01  A
10:      0.10592      2.88216      0.1068E-06    0.2597E-01  A
11:      0.10753      2.92604      0.1321E-06    0.2037E-01  A
12:      0.10753      2.92604      0.3438E-08    0.7829     A
13:      0.10753      2.92604      0.3785E-08    0.7112     A
14:      0.11237      3.05776      0.7005E-01    0.3518E-07  A
15:      0.11321      3.08072      0.7619E-01    0.3187E-07  A
16:      0.11327      3.08233      0.6733E-08    0.3603     A
17:      0.11327      3.08233      0.3842E-07    0.6314E-01  A
18:      0.11327      3.08234      0.4878E-03    0.4972E-05  A
19:      0.11537      3.13932      0.2435E-02    0.9605E-06  A
20:      0.12095      3.29119      0.1663E-01    0.1279E-06  A
```

Recalling the spin-forbidden transitions appear with near vanishing oscillator strengths in an SOC treatment, we note the following from these results:

- Excitation no. 7 is the lowest with a relevant oscillator strength f, it corresponds to $S_0 \rightarrow S_1$.
- The $S_0 \rightarrow S_1$ excitation energy of 2.77 eV compares well with the experiment value, 2.85 eV.
- At the GS geometry the T_1 and the T_2 state lie below S_1.

Computational Description of TADF 2: Spin-Orbit Coupling

As discussed above, transitions between S and T states are formally forbidden within a non-relativistic framework. Phosphorescence or intersystem crossings thus become only possible due to the presence of spin-orbit coupling (SOC) effects. Compared to other interactions these couplings are typically small and can therefore be treated as a perturbation of the systems electronic structure mediated by $\hat{H}_{\mathrm{SOC}}$, the SOC operator. There exist various different approaches and approximation for $\hat{H}_{\mathrm{SOC}}$. See the recent review of Marian for an overview of spin-orbit methods in the context of excited states electronic structures and intersystem crossing rates.

In this case Fermi's golden rule provides an expression for the reversed intersystem crossing rate

$$k_{\mathrm{RISC}} = \frac{2\pi}{\hbar} |V_{\mathrm{SOC}}|^2 \times \rho_{\mathrm{FCWD}}$$

which will be used in the following. $|V_{\mathrm{SOC}}|^2$ is directly proportional to k_{RISC} and is to be understood as coupling term of the matrix representation of $\hat{H}_{\mathrm{SOC}}$. We model the transition from T_1 to S_1, whereas T_1 actually consists of three individual states the system can assume;

⬤SCM

$$|V_{\mathrm{SOC}}|^2 = \frac{1}{3} \left| \left\langle S_1 \left| \hat{H}_{\mathrm{SOC}} \right| T_1 \right\rangle \right|^2 = \frac{1}{3} \sum_{J=-1,0,1} \left\langle S_1 \left| \hat{H}_{\mathrm{SOC}} \right| T_1^J \right\rangle \left\langle S_1 \left| \hat{H}_{\mathrm{SOC}} \right| T_1^J \right\rangle^*$$

As $|V_{\mathrm{SOC}}|^2$ is strongly affecting the reverse intersystem crossing rate, developing novel TADF emitters with larger SOCME values is an important part of many OLED related research activities.

The other important factor entering the k_{RISC} rate is ρ_{FCWD}, the Frank-Condon-weighted density of states, which will be addressed in the corresponding section below.

Calculating Spin-Orbit Couplings

The reverse intersystem crossing process itself occurs on a too short timescale for the systems geometry to readapt during the $T_1 \rightarrow S_1$ transition. The factor $|V_{\mathrm{SOC}}|^2$ in the above expression for k_{RISC} is therefore computed at the optimized geometry of the T_1 state.

Open a new instance of ADFinput

Load the previously optimized T1 structure with **File → Import Coordinates...**

In the **Main** panel:

Task: → Single Point

XC-Functional → Range Separated → LCY PBE

Click on the **...** button left of the **XC-Functional** field

Enter **Gamma:** 0.22

Return to **Main** panel

Relativity → Scalar

Basis set → TZP

Frozen core → None

Numerical quality → Good

Click on **Model** panel and select **Solvation**

Solvation method: → COSMO

COSMO solvent → Toluene

Click on **Details** panel and select **COSMO**

Enable **Include response in TDDFT**

Click on **Properties** and select **Excitations (UV/Vis), CD**

Type of excitations: → Spin-Orbit (Perturbative)

TDA: → Yes

Number of excitations: 5

Calculate: → NTOs

SCM

❗ **See also**

- 📥 4CzIPN_SOCME.run run script to compute the spin-orbit coupling matrix elements

After the calculation is completed, open the output file with ADFoutput. In the ADFoutput the SOCME results can be found with **Response Properties → Spin-orbit couplings**:

```
Spin-orbit couplings calculated as root mean squares: square root
of (the sum of squares of spin-orbit coupling matrix elements of
all sublevels of the uncoupled states) in cm-1
                   T1        T2        T3        T4        T5
                 -------   -------   -------   -------   -------
<S|Hso|T>
---------
       S1:        0.40      1.07      0.35      0.17      2.17
       S2:        0.89      0.40      1.67      1.14      0.16
       S3:        0.05      1.43      0.17      0.29      0.66
       S4:        0.09      1.72      0.25      0.18      0.88
       S5:        0.30      0.09      0.61      0.49      0.02
<T|Hso|T>
---------
       T1:        0.00      1.24      0.13      0.27      3.31
       T2:        1.24      0.00      2.15      2.05      0.21
       T3:        0.13      2.15      0.00      0.44      0.44
       T4:        0.27      2.05      0.44      0.00      1.18
       T5:        3.31      0.21      0.44      1.18      0.00
```

From the $|\langle S_1 | \hat{H}_{\mathrm{SOC}} | T_1 \rangle|$ value of 0.4 cm^{-1} we then obtain $|V_{\mathrm{SOC}}|^2 = 8.2 \cdot 10^{-10}$ eV^2.

Computational Description of TADF 3: Vibrations

Recall the aforementioned expression for the reverse intersystem crossing rate:

$$k_{\mathrm{RISC}} = \frac{2\pi}{\hbar} |V_{\mathrm{SOC}}|^2 \times \rho_{\mathrm{FCWD}}$$

While $|V_{\mathrm{SOC}}|^2$ can be interpreted as probability for the $T_1 \rightarrow S_1$ transition, ρ_{FCWD} describes the thermokinetic barrier associated with this process.

Semiclassical Marcus Theory

Semiclassical Marcus theory (SCMT) provides a simple way to describe this thermokinetic barrier. The potential energy surfaces of both states around their respective minimum structures are thereby described in terms of parabolic functions.
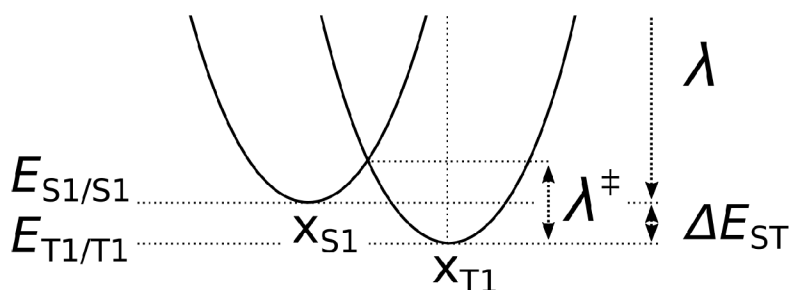
Fig. 15 Potential energy surfaces of the S_1 and T_1 states as quadratic functions centered at x_{S1} and x_{T1}, respectively. In Marcus theory the difference between $E_{S1/S1}$ and $E_{S1/T1}$ is used to estimate the thermokinetic barrier of the $T_1 \to S_1$ transition.

Assuming the same curvature of both states, i.e. $E(T_1) = a \cdot x^2$ and $E(S_1) = a \cdot (x + x_{S1} - x_{T1})^2 + \Delta E_{ST}$, one finds the for the $T_1 \to S_1$ barrier height as the intersection of both parabolas:

$$\lambda^{\ddagger} = \frac{(\Delta E_{ST} + \lambda)^2}{4\lambda}$$

Using this barrier height in an Arrhenius-type expression yields then the RISC rate:

$$\rho_{FCWD}^{SCMT} = \frac{1}{\sqrt{4\pi\lambda k_B T}} \exp\left(-\frac{(\Delta E_{ST} + \lambda)^2}{4\lambda k_B T}\right)$$

The reorganization energy λ can thereby be considered as the energy required to bring the system in the S_1 to the minimum structure of the T_1 state. Designating the energies of the S_1 state at x_{S1} and x_{T1} as $E_{S1/S1}$ and $E_{S1/T1}$, respectively, on can use

$$\lambda = E_{S1/T1} - E_{S1/S1}$$

to calculate k_{RISC}. We can thereby set up the necessary calculations analogously to the vertical absorption calculations:

Open a new instance of ADFinput

Load the previously optimized S1 structures with **File → Import Coordinates...**

In the **Main** panel:

Task: → Single Point

XC-Functional → Range Separated → LCY PBE

Click on the **...** button left of the **XC-Functional** field

Enter **Gamma:** 0.22

Return to **Main** panel

Frozen core → None

Numerical quality → **Good**

Click on **Model** panel and select **Solvation**

Solvation method: → **COSMO**

COSMO solvent → **Toluene**

Click on **Details** panel and select **COSMO**

Untick **Include response in TDDFT**

Click on **Properties** and select **Excitations (UV/Vis), CD**

Type of excitations: → **Spin-Orbit (Perturbative)**

TDA: → **Yes**

Number of excitations: 5

Calculate: → **NTOs**

Calculate: → **Charge transfer descriptors**

Save the input **File** → **Save as...** under e.g. *4CzIPN_S1_S1.adf*

Analogously for the S1/T1 calculation we set:

Load the previously optimized T1 structures with **File → Import Coordinates...**

Repeat the above steps

Save the input **File** → **Save as...** under e.g. *4CzIPN_S1_T1.adf*

❶ See also

- ⬇ 4CzIPN_S1atS1.run run script to compute $E_{S1/S1}$
- ⬇ 4CzIPN_S1atT1.run run script to compute $E_{S1/T1}$

After running the calculations the required energies can be extracted again with ADFoutput. Note, that the excited states energies are obtained from the ground state energy and the respective excitation energies. These can be retrieved in ADFoutput as *Total Bonding Energy* under **Properties → Bonding Energy Decomposition** and as the first excitation with a significant oscillator strength under **Response Properties → All Spin-Orbit Coupling Excitation Energies**, respectively.

For 4CzIPN this results in a value of $\lambda = E_{S1/T1} - E_{S1/S1}$ = 0.06 eV. This result can now be used along with the previously obtained values ΔE_{ST} = 0.16 eV and $|V_{SOC}|^2 = 8.2 \cdot 10^{-10}$ eV^2 in the above expressions for ρ_{FCWD}^{SCMT} and k_{RISC}.

Compared to that, Samanta et al. obtained higher rates for 4CzIPN ($4.9 \cdot 10^6$ – $1.8 \cdot 10^7$/ s). This difference can be rationalized by their usage of different DFT approximations, the significantly smaller value of ΔE_{ST} obtained thereby, and a different handling of the spin-orbit couplings. We also note that Samanta et al. argued that for emitters like 4CzIPN λ can be replaced with an effective value between 0.1 and 0.2 eV. When using λ = 0.1 eV instead of the previously calculated reorganization energy, the RISC rate rises to k_{RISC} = $6.3 \cdot 10^5$ / s.

Franck-Condon Principle and Marcus-Levich-Jortner Theory

While the semiclassical often provides acceptably accurate results, it relies on some strong assumptions and the real situation turns out more intricate: First, the potential energy surfaces around both minima are described by the entirety of vibrational normal modes. Each normal mode defines a separate harmonic oscillator system which, in a quantum mechanical description, leads to a separate set of vibrational eigenfunctions (quanta). The Franck-Condon principle then states that the $T_1 \rightarrow S_1$ transition requires a significant overlap between nuclear wavefunctions of both electronic states.
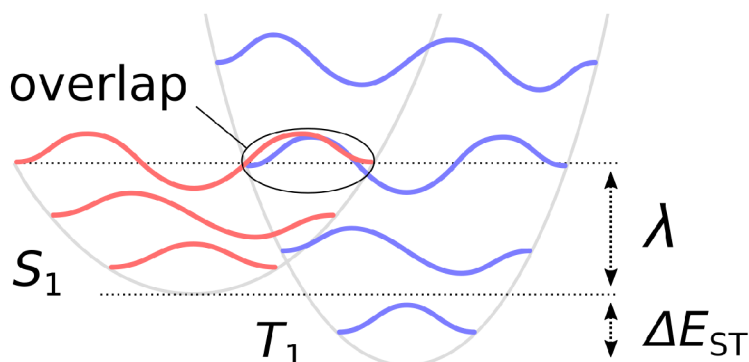
Fig. 16 The Franck-Condon principle describes $T_1 \rightarrow S_1$ transition rate in terms of the overlap between the nuclear vibronic wavefunctions of the initial and final state, respectively.

One can distinguish between two limiting cases: the quanta low frequency vibrations from shallow modes and from rearranging solvent molecules (see below) typically form an essentially continuous spectrum. Pairs of overlapping quanta from low frequency modes will therefore occur at energies close to the intersection of the two parabolic potential curves, which is leads to results equivalent to those of semiclassical Marcus theory. Within semiclassical Marcus theory the effect of these modes can be described in terms of a Marcus reorganization energy λ_{M}. If the transition is dominated by high frequent modes, nuclear tunneling effects and the overlap of individual pairs of quanta are prevalent. The effect of such modes consists mainly in a renormalization of the coupling parameters.

An extension of SCMT, Marcus-Levich-Jortner theory includes includes both of these limiting

SCM

$$\rho_{\mathrm{FCWD}}^{\mathrm{MLJT}} = \frac{1}{\sqrt{4\pi\lambda_{\mathrm{M}}k_{\mathrm{B}}T}} \sum_{n=0}^{\infty} \exp(-S_{eff}) \frac{S_{eff}^n}{n!} \exp\left(-\frac{(\Delta E_{\mathrm{ST}} + n\hbar\omega_{eff} + \lambda_{\mathrm{M}})^2}{4\lambda_{\mathrm{M}}k_{\mathrm{B}}T}\right)$$

Thereby, S_{eff} denotes the Huang-Rhys factor of this effective mode, which is a measure for the strength of the electron-phonon coupling. S_{eff} and the corresponding frequency ω_{eff} are obtained from the Huang-Rhys factors and frequencies of the individual high frequency normal modes.

$$S_{eff} = \sum_i S_i \qquad \omega_{eff} = \sum_i \frac{\omega_i S_i}{S_{eff}}$$

Whereas modes with $\omega_i > 1000$ cm^{-1} are typically included in the summation.

Samanta et al. computed S_i factors from mode resolved reorganization energies $\lambda_i = k_i \Delta Q_i^2 / 2$, which in turn results from the frequencies $k_i = \omega_i^2$ and ΔQ_i, the normal mode projection onto the transition path.

For a large emitter molecule like 4CzIPN however, the calculation of the full Hessian matrix turns out computationally too expensive.

Effective Modes and Huang-Rhys Factors from DFTB and FCF

In some cases, the DFTB method can be used as a more approximate but efficient alternative to compute the normal modes. The FCF program of the Amsterdam Modeling Suite can then be used to calculate the S_i factors which then lead to the S_{eff} and ω_{eff} values. The following procedure illustrates how this can be achieved with the Amsterdam Modeling Suite.

> ❶ **Warning**
>
> The calculation of Huang-Rhys factors crucially depends on the quality of the normal modes. Their computation from TD-DFTB excited states gradient must be carefully tested to determine their validity for a given dye system.

Open a new instance of ADFinput

Load the previously optimized S_1 structure via **File → Import Coordinates**

In the options panel click **ADF** → **DFTB**

Task: → Geometry Optimization

Followed by: → Frequencies

SCM

Properties → Excitations (UV/Vis)

Type of excitations: → Singlet

Method: → Davidson

Number of excitations: → 2

Analogously, for the T_1 state:

Open a new instance of ADFinput

Load the previously optimized T_1 structure via **File → Import Coordinates**

...

Properties → Excitations (UV/Vis)

Type of excitations: → Triplet

Method: → Davidson

Number of excitations: → 2

❶ See also

- ⬇ 4CzIPN_optFreqDFTB_S1.run DFTB optimization and normal modes on S_1
- ⬇ 4CzIPN_optFreqDFTB_T1.run DFTB optimization and normal modes on T_1

After completing both calculations, the binary result files *dftb.rkf* containing the normal modes are found in the respective directories *<jobname>.results*. Create a new directory and copy these rkf files naming them e.g. *S1_optFreqDFTB.rkf* and *T1_optFreqDFTB.rkf*. Based on these results the program-tool *fcf* can be invoked to compute S_{eff} and ω_{eff} values using the following bash script:

```
$ADFBIN/fcf << eor
STATES T1_optFreqDFTB.rkf S1_optFreqDFTB.rkf
QUANTA 0 0
TRANSLATE
ROTATE
eor
```

Running this script yields the frequencies and Electron-Phonon couplings for both states as shown in the following example:

SCM

```
  Frequency          Displacement  Electron-Phonon coupling
    cm^-1             a0 amu^1/2        (dimensionless)
 ----------          ----------        ----------
   12.070318         -11.804599          2.642917
   13.872303           3.368437          0.808492
   19.113716          -2.303894          0.649094

   ...
  976.643338          -0.001580          0.003183
  986.370540          -0.000023          0.000046
 1041.616941          -0.001475          0.003069
 1075.333767          -0.019010          0.040172
 1078.281693          -0.017297          0.036603

   ...
 3075.114508           0.033650          0.120250
 3086.236558           0.013900          0.049764
 3087.310659           0.005134          0.018383


   ...
```

We are interested in the $T_1 \rightarrow S_1$ transition and are therefore using the results from the first state. The mode-resolved Huang-Rhys factors S_i are obtained as the square of the above Electron-Phonon coupling parameters. Using the above expressions for S_{eff} and ω_{eff}, we then sum over all modes with $\omega_i > 1000$ cm^{-1}. This results in S_{eff} = 0.837 and ω_{eff} = 1498 cm^{-1}.

These quantities are then used in the above expression for $\rho_{\mathrm{FCWD}}^{\mathrm{SCMT}}$ (with $\lambda_{\mathrm{M}} = \lambda$ = 0.06 eV) whereas the summation is stopped at n = 5. With $|V_{\mathrm{SOC}}|^2 = 8.2 \cdot 10^{-10}$ eV^2 this results in a reverse intersystem crossing rate that is essentially identical to the result from semiclassical Marcus theory of k_{RISC} = 2.3·10^5 / s. This supports the finding of Samanta et al. that quantum tunneling effects are negligible in the reverse intersystem crossing process of 4CzIPN and that a classical treatment suffices for its description.

Computational Description of TADF 4: Solvent Effects

The approach presented above included solvent effects implicitly, as the COSMO model was used in the calculations.

Besides examining vibrational modes that simultaneously involve both, the OLED emitter and explicit solvent molecules, and pursuing analogously to the approach for intramolecular vibrations discussed above, many more explicit treatments have been suggested in the literature. Outersphere vibronic contributions can for example be obtained in terms of dielectric response functions (Rühle et al.), polarizable force fields (McMahon and Troisi), or from QM/MM approaches (Norton and Brédas).